

https://dspace.org/

The effects of supplementary cementing materials in modifying the heat of hydration of concrete

Ballim, Yunus; Graham, Peter C.

2008-09-23
http://hdl.handle.net/10539/11198

Downloaded from a DSpace repository. https://dspace.org/

Materials and Structures (2009) 42:803–811
DOI 10.1617/s11527-008-9425-3

ORIGINAL ARTICLE

The effects of supplementary cementing materials in modifying the heat of hydration of concrete

Yunus Ballim · Peter C. Graham

Received: 23 February 2008 / Accepted: 17 September 2008 / Published online: 23 September 2008
© RILEM 2008

Abstract This paper is intended to provide guidance on the form and extent to which supplementary cementing materials, in combination with Portland cement, modifies the rate of heat evolution during the early stages of hydration in concrete. In this investigation, concretes were prepared with fly ash, condensed silica fume and ground granulated blast-furnace slag, blended with Portland cement in proportions ranging from 5% to 80%. These concretes were subjected to heat of hydration tests under adiabatic conditions and the results were used to assess and quantify the effects of the supplementary cementing materials in altering the heat rate profiles of concrete. The paper also proposes a simplified mathematical form of the heat rate curve for blended cement binders in concrete to allow a design stage assessment of the likely early-age time–temperature profiles in large concrete structures. Such an assessment would be essential in the case of concrete structures where the potential for thermally induced cracking is of concern.

Keywords Heat of hydration · Fly ash · Silica fume · Slag · Concrete

Y. Ballim (✉) · P. C. Graham
School of Civil & Environmental Engineering, University of the Witwatersrand, Private Bag 3, WITS 2050, Johannesburg, South Africa
e-mail: yunus.ballim@wits.ac.za

1 Introduction

Supplementary cementing materials, such as ground granulated blastfurnace slag (GGBS), fly ash (FA) and condensed silica fume (CSF), are now routinely used in structural concrete. Used judiciously, these materials are able to provide improvements in the economy, microstructure of cement paste as well as the engineering properties and durability of concrete. They also alter the rate of hydration and can influence the time–temperature profile in large concrete elements.

This paper is aimed at an improved understanding of the way in which the early-age heat of hydration characteristics of concrete are altered by the addition of supplementary cementing materials (SCM), in combination with Portland cement, as a part of the binder. Importantly, in the design and construction of large concrete elements, where the extent of temperature rise is of concern, our ability to reliably predict the early-age temperature differentials in the concrete requires a careful understanding of the rates at which heat is evolved during hydration [1–3]. In essence, the intention of this paper is to provide guidance on the form of the heat-rate function for concretes containing supplementary cementing materials. This is essential input information in the design and construction of large dimension and/or high strength structures where thermal strains are likely to lead to deleterious cracking and/or loss of durability.

In the investigation reported here, concrete samples containing combinations of Portland cement with

GGBS, FA or CSF were tested in an adiabatic calorimeter in order to determine their heat of hydration characteristics. The test programme was limited to binary blends of the materials, i.e., each test was limited to a combination of Portland cement and one supplementary material and all concretes were prepared at the same water:binder (w/b) ratio. For each type of supplementary material, concretes were prepared with supplementary material replacing between 5% and 80% of the Portland cement, depending on the type of SCM.

Concrete samples with a volume of approximately 1 l were tested in the adiabatic calorimeter. The adiabatic calorimeter that was used in the test programme is based on the principle of surrounding a concrete sample with an environment in which the temperature is controlled to match the temperature of the hydrating concrete itself, thus ensuring that no heat is transferred to or from the sample and the rise in temperature measured is solely due to the heat evolved by the hydration process. This calorimeter has been described in detail by Gibbon et al. [4].

Since the rate of evolution of heat during the hydration of cementitious materials is influenced by the temperature at which the reaction takes place, there is no unique adiabatic heat rate curve for a particular cement or combination of cementitious materials. Comparisons of the heat rate performances of materials must, therefore, be made on the basis of the degree of hydration or maturity. In this paper, the results are expressed in terms of maturity or t_{20} h, which refers to the equivalent time of hydration at 20°C. This form of expression of the heat rate function and the justification for its use, is described by Ballim and Graham [1].

2 Concrete materials and mixtures

Concrete materials which are commonly used and readily available in South Africa were used in these tests. The Portland cement complied with SABS EN 197-1, type CEM I class 42.5 [5] and the GGBS, fly ash and silica fume complied with SABS 1491 Parts 1, 2 and 3 [6–8], respectively. The oxide contents of the binder materials were determined by XRF analysis and the results are shown in Table 1.

The range of replacement levels by each of the three supplementary materials used, together with the concrete mixture proportions, is shown in Table 2. The concrete mixture proportions were kept the same throughout, except that the composition and relative proportion of the binder was changed as required. All the concretes therefore had a w/b ratio of approximately 0.67 and the water content was sufficient to compact the concrete by manually stamping the sample holder. All the mixture components, including the water, were stored in the same room as the calorimeter at least 24 h before mixing. This allowed the temperature of the materials to equilibrate to the room temperature, which was controlled at 19 ± 1°C. A 1.2 l sample of each concrete was prepared by

Table 1 Chemical analyses (%) of the binder materials used in adiabatic calorimeter tests

	CEM I	GGBS	Fly ash	CSF
SiO_2	22.9	36.4	55.1	89.4
Al_2O_3	4.6	14.8	33.3	2.0
Fe_2O_3	2.58	0.98	3.15	2.03
Mn_2O_3	0.12	1.24	0.02	0.16
TiO_2	0.46	0.71	1.67	0.08
CaO	64.0	34.3	4.2	0.7
MgO	1.6	9.7	1.2	0.5
P_2O_5	0.06	0.00	0.39	0.14
SO_3	2.05	2.34	0.12	0.18
K_2O	0.30	0.87	0.69	1.09
Na_2O	0.12	0.34	0.00	0.12
LOI	2.41	−0.92	0.45	3.82
Total	100.0	100.8	100.2	100.3

Table 2 Mixture proportions (kg/m^3) of the concretes tested

Mix	CEM I	CSF	GGBS	Fly ash	Water	Sand	Stone
100% Cem I	350	0	0	0	233	885	850
5% CSF	332.5	17.5	0	0	233	885	850
10% CSF	315	35	0	0	233	885	850
15% CSF	297.5	52.5	0	0	233	885	850
20% GGBS	280	0	70	0	233	885	850
40% GGBS	210	0	140	0	233	885	850
60% GGBS	140	0	210	0	233	885	850
80% GGBS	70	0	280	0	233	885	850
20% FA	280	0	0	70	233	885	850
40% FA	210	0	0	140	233	885	850
60% FA	140	0	0	210	233	885	850
80% FA	70	0	0	280	233	885	850

manual mixing in a steel bowl and the adiabatic test was started within 15 min after the water was added to the mixture. All the tests were started at temperatures between 18 and 20°C and temperature measurement in the calorimeter was continued for approximately 4 days.

The silica sand used in the concretes was obtained in three size fractions and these were recombined as needed for the mixing operation to ensure a uniform sand grading for each concrete. The stone used in the concrete was a washed silica, largely single-sized and 9.5 mm in nominal dimension.

3 Results and discussion

3.1 Heat rate measurements

The adiabatic calorimeter results from the tests on the GGBS, FA and CSF concretes are shown in Figs. 1, 2 and 3, respectively. The results are shown for the first 100 t_{20} h of the test and the heat rates are expressed as Joules per "maturity second" per kg of binder. In the figures, this is referred to as a "maturity heat rate". Table 3 presents details of the peak heat rates (q_{max}) as determined from the results shown in Figs. 1–3. To provide a basis for comparison and to highlight the hydration effect of the SCM in the binder, Table 3 also shows the peak heat rates normalised to 100% CEM I.

Figure 4 shows how the peak heat rates vary with a change in the proportions of SCM in the binder. This figure also shows trend lines for the results of the different SCM types. The sections which follow present a more detailed discussion of the relative performance of the different binder types.

3.2 GGBS binders

Figure 1 shows that the peak hydration heat rate decreases as the proportion of GGBS in the sample is increased. Table 3 shows that the time to reach this peak hydration rate is marginally reduced as the proportion of GGBS is increased to 60%. However, the reduction in the time to peak heat rate is more significant as the proportion of GGBS is increased from 60% to 80%.

Table 3 also shows that the normalised peak heat rates for the GGBS concretes are higher than that of the plain CEM I concrete. This indicates that the hydration of the GGBS is contributing to the generation of heat in the concrete, even at these relatively early ages. An analysis of the results obtained by Wu et al. [9] shows a similar response by the GGBS concretes that they tested.

Figure 4 shows a linear relationship between the peak heat rate and proportion of the CEM I in the concretes containing GGBS. From this figure, the empirical relationship between the peak heat rate and the proportion of GGBS in the concrete is as shown in Eq. 1, together with the correlation coefficient, R^2.

$$q_{max} = 0.0263(C) + 0.23 \quad [R^2 = 0.997] \qquad (1)$$

where q_{max} is the peak heat rate and C is the percentage of CEM I in the GGBS binder blend.

Further to the point made above regarding the early hydration of the GGBS, Eq. 1 suggests that, on a maturity time basis, the background contribution

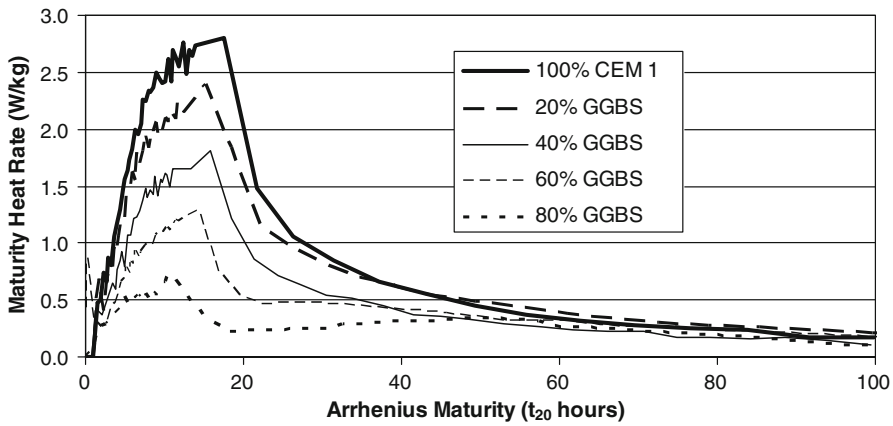


Fig. 1 Heat rate profiles for the concretes containing CEM I and GGBS

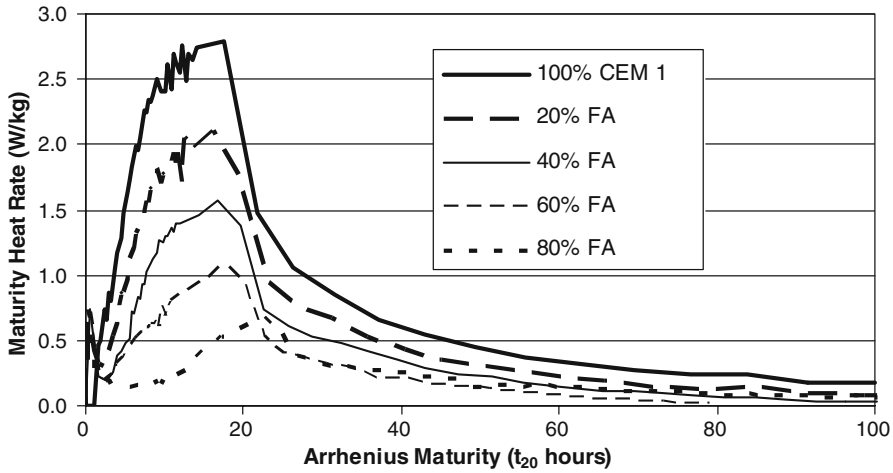


Fig. 2 Heat rate profiles for the CEM I and FA concretes

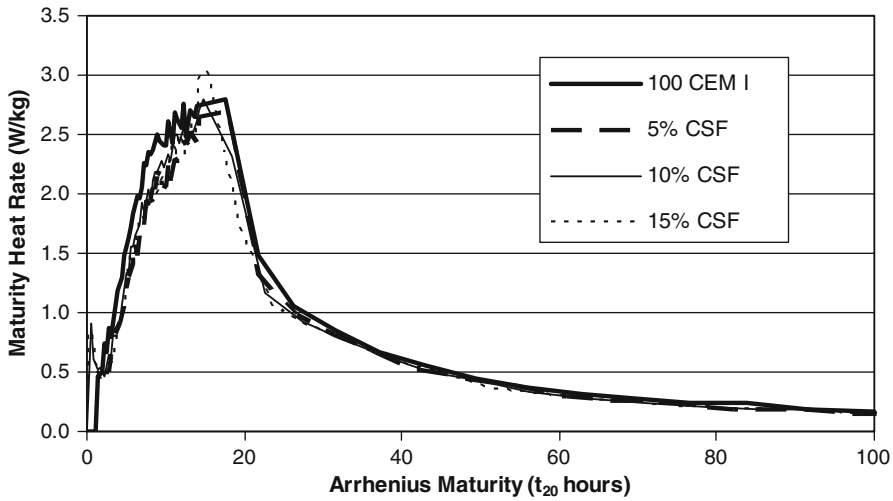


Fig. 3 Heat rate profiles for CSF concretes

of GGBS to the peak heat rate is 0.23 W/kg. However, this value should not be read as the peak heat rate for GGBS on its own since, even at this early stage, it can be expected that some activation of the GGBS has occurred because of the presence of the CEM I and its hydration products. This acceleration effect of the GGBS on the hydration of CEM I was noted by Escalante-Garcia and Sharp [10] and supported by Zhou et al. [11] who ascribe the phenomenon to the 'dilution effect' (more water available to the CEM I), the consumption of calcium hydroxide by the GGBS and the GGBS particles acting as nucleation sites for the formation of calcium hydroxide.

Another feature of the GGBS concrete heat rate curves shown in Fig. 1 is that, at GGBS replacements of 60% and 80%, there is a second acceleration of the rate of heat evolution. This acceleration starts at around 20 t_{20} h and peaks at around 50 t_{20} h. This is likely to be caused by a later stimulation of hydration activity of the GGBS, a feature that was also noted by Wu et al. [9] and by Zhou et al. [11]. In the case of the concretes with lower levels of GGBS replacement, the onset of the GGBS hydration overlaps with the decline in the rate of CEM I hydration because of the higher temperatures reached by the concrete in the adiabatic test as well as the higher levels of GGBS hydration activation from the products of CEM I hydration. Higher temperatures have a significant effect in stimulating the hydration of GGBS in Portland cement [12]. Since lower temperatures are achieved in the adiabatic test of the concretes with higher levels of GGBS in the binder, the hydration rate peaks of the CEM I and the GGBS are separated

Table 3 Assessment of the peak heat rate characteristics of the GGBS concretes

Binder composition	Time to q_{max} (t_{20} h)	q_{max} (W/kg)	q_{max} normalised to 100% CEM I (W/kg)
100% CEM I	17.6	2.80	2.80
20% GGBS	15.3	2.39	2.99
40% GGBS	15.7	1.81	3.02
60% GGBS	14.2	1.30	3.25
80% GGBS	10.7	0.73	3.65
20% FA	16.2	2.11	2.64
40% FA	16.8	1.57	2.62
60% FA	17.4	1.07	2.67
80% FA	22.0	0.70	3.50
5% CSF	17.9	2.71	2.85
10% CSF	14.8	2.80	3.11
15% CSF	15.3	3.05	3.59

3.3 Fly ash binders

The adiabatic calorimeter results obtained from the FA binder mixes are shown in Fig. 2. This figure shows that the heat rate curves for the FA binders behave similarly to those for the GGBS binders in that the peak heat rates reduce with increasing FA in the binder. Table 3 shows an analysis of the peak heat rates for the FA concretes, together with the normalised peak heat rates on the assumption of 100% CEM I binder.

Table 3 shows that replacement of 20% and 40% of CEM I with FA in the binder cause a small acceleration in the time required to reach the peak heat rate. On the other hand, a replacement of 80% resulted in a significant retardation of the hydration activity in comparison with the plain CEM I concrete. At the higher levels of FA replacement,

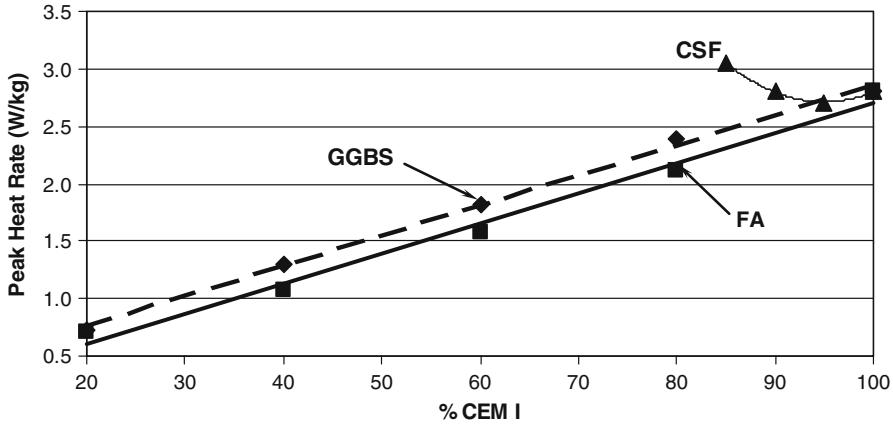


Fig. 4 Variation in the peak heat rate with different proportions of GGBS, FA and CSF in the concrete binder

and more clearly distinguished in the curves shown in Fig. 1. Nevertheless, where the rates of heat evolution of the 60% and 80% GGBS concretes exceed those of the lower GGBS content concretes, this occurs at later ages, at relatively low measured heat rates and the differences are marginal.

As noted earlier and shown in Table 3, increasing proportions of GGBS in the binder between 20% and 60%, have the effect of marginally reducing the time to the peak rate of heat evolution. This is possibly explained by the hydration activity of the GGBS together with a dilution of the effect of the gypsum in the Portland cement. The reduced retardation effect of the SO_3 on the hydration of the CEM I would then manifest in an earlier peak rate of hydration.

this observation is in agreement with that found by Maekawa et al. [3], who note that the addition of fly ash to a binder delays the start of active hydration. This delay period is particularly noticeable in the heat rate curve of the 80% FA concrete, as shown in Fig. 2. A study undertaken by Fajun et al. [13] using FA replacements of 40%, showed retardation effects as being from marginal for low-lime FA to a more than doubling in the time to achieve the peak heat rate for high-lime FA.

The FA used in this study (see Table 1) would be classified as a low-lime FA (CaO content of 4.2%) but it differs from the FA used by Fajun et al. [13] in having a significantly lower Fe content (3.15% compared to 17.3%) as well as a lower alkali metal

content (sodium + potassium content of 0.69% compared with 2.28%). However, notwithstanding these chemical composition differences, Fajun et al. [13] draw the important conclusion that the retardation effect appears to be more strongly influenced by the nature and condition of the surfaces of the FA. While the observed acceleration effect of the FA, as shown in Table 3, may well be a feature of its surface characteristics, this aspect was not studied in this investigation.

Table 3 also shows that, when the peak heat rate is normalised to 100% CEM I, the presence of up to 60% FA has the effect of reducing the rate of hydration activity of the Portland cement. However, at 80% replacement with FA, the normalised peak heat rate is higher than that of the plain CEM I concrete. While the reduced normalised heat rate is a feature of the later hydration of the FA [13], it is not clear why the effect should be reversed in the case of the 80% FA replacement. Again, this may relate to the physico-chemical characteristics of the FA used in this study.

As in the case of the GGBS concretes, Fig. 4 shown a near-linear relationship between the peak rate of heat evolution and the proportion of CEM I in the binder of the FA concretes. Equation 2 shows the form of the straight line fitted to the measured results for the FA concretes as shown in Fig. 4. The variables are as described for Eq. 1.

$$q_{\max} = 0.0262(C) + 0.078 \quad \left[R^2 = 0.988\right]. \tag{2}$$

Accounting for the lower correlation coefficient of the line fitted to the FA results, a comparison between Eqs. 1 and 2 (and Fig. 4) show that the slopes of the two lines are almost equal. On the other hand, the FA line in Eq. 2 is shifted downward to a near-zero rate of hydration for the 0% CEM I content, as to be expected of fly ash on its own. However, the similarity of the slopes of Eqs. 1 and 2 indicates that, because of the low hydration activity of both GGBS and FA at the early ages considered in this study, the rate of heat evolution of the concretes tested is dominated by the hyrdration of the CEM I in the binder, regardless of the level of replacement. Furthermore, this result seems to imply that the 'dilution effect' presented by other researchers [10, 11] is not a predominant factor in this series of tests. If a dilution phenomenon is indeed operative, its effect is stimulating the hydration of the CEM I is small, as indicated by the offset value of 0.078 in Eq. 2.

3.4 Condensed silica fume binders

The adiabatic calorimeter results for the CSF sample tests are shown in Fig. 3. This Figure indicates that replacing up to 15% of CEM I with CSF has a relatively small effect on the heat-rate profile as well as the peak rate of heat of the concrete. Table 3 also shows an analysis of the peak heat rate characteristics of the CFS concretes.

While the effects do not appear to be very large, Fig. 3 and Table 3 show that the important differences between the heat-rate profiles of the plain CEM I concrete and those of the CSF concretes are:

- The duration of the peak heat rate of the CSF concretes is significantly shortened as the CSF content increases above 5%.
- At CSF replacement rates of 10% and 15%, the time to reach the peak rate of heat evolution is noticeably accelerated.
- At a 15% CSF replacement, the peak rate of heat evolution is increased by approximately 9% over that of the plain CEM I concrete.

Furthermore, the effectiveness of CSF in stimulating the hydration of Portland cement is illustrated by the significant increase in the peak rate of heat evolution when normalised to 100% CEM I, as shown in Table 3.

Figure 4 also shows the variation of the measured peak heat rate as the proportion of CSF in the binder is varied. Equation 3 shows the form of the curve fitted to the measured results for the CSF concretes as shown in Fig. 4. The variables are as described for Eq. 1.

$$q_{\max} = 0.0034C^2 - 0.646C + 33.38 \quad \left[R^2 = 0.9997\right]. \tag{3}$$

The very good fit of Eq. 3 to the measured data for CSF concretes ($R^2 = 0.9997$) may well be misleading. The reduced hydration activity at 5% CSF content in the binder is not easily explained and this would require further assessment, perhaps using different measurement techniques, to confirm this observation. Also, some caution is necessary in extrapolating this curve to CSF contents higher than 15% as it is likely

that an optimum point will be reached, beyond which the rate of hydration should decline because of a diminishing availability of calcium hydroxide in the mixture. Nevertheless, the curve is useful in providing guidance on the likely effect of the addition of CSF on the hydration of CEM I at these relatively modest levels of replacement.

3.5 Effect of SCM on early hydration of blended cements

In the case of the GGBS and FA concretes, the linear relationship between the peak heat rates and the proportion of CEM I in the blend appears to indicate that, at these early stages of hydration, the hydration of the binder is dominated by the CEM I and, such evidence of pozzolanic reaction activity as there may be, is masked by the CEM I hydration. The time scale involved in the results presented here is the equivalent of approximately 5 days of hydration at 20°C. The effect of the presence of these SCM's appears rather to lie in stimulating the hydration of the CEM I through the dilution effect, consumption of calcium hydroxide and provision of nucleation sites for stimulating hydration [10, 11].

In the case of CSF as an SCM, the increase in the peak rates of hydration of the concretes tested is most likely to be explained by the efficient nucleation site effect of this material in stimulating the hydration of the CEM I. This may well explain the observed increase in the peak hydration rate with increasing CSF content in the blend. It is our view that the effects of any pozzolanic reaction of the CSF are not clearly evident in the early-age results presented here.

4 A proposed design approach

In the design of concrete elements where the development of thermal strains and possible cracking stresses are of concern, it is necessary to reliably predict the early-age temperature development in the structure. Such structures would range from very large, low strength, mass concrete elements to structural elements, of more modest dimension but with high binder contents or high strength expectations. In these cases, the temperature prediction will usually be based on a solution of Eq. 4, which is the Fourier equation for heat transfer in three dimensions (see for example, Refs. [14, 15]).

$$\rho \cdot C_p \cdot \frac{\partial T}{\partial t} = k\left(\frac{\partial^2 T}{\partial x^2} + \frac{\partial^2 T}{\partial y^2} + \frac{\partial^2 T}{\partial z^2}\right) + \frac{\partial q}{\partial t}(t) \qquad (4)$$

where: ρ = density of the concrete; C_p = the specific heat capacity of the concrete; T = temperature; t = time; k = thermal conductivity of the concrete; x, y and z are the coordinates at a particular point in a structure and $\frac{\partial q}{\partial t}(t)$ is the time rate of heat evolution by the hydrating cement at point (x, y, z) in the structure.

Such an analysis will require as input information, a reasonable estimate of the time-based rate of heat evolution profile of the binder to be used in the concrete. This section presents a simplified approach to determining the maturity heat rate function, $\frac{\partial q}{\partial M}(t)$, for concretes containing blends of CEM I with GGBS, FA or CSF as the binder. This approach should be used in the absence of a more reliable measure of the heat-rate function and should be considered only as a reasonable first estimate of the actual heat rate function. It should be noted that, at each point in the concrete element and at each different time interval, the time-based heat rate is determined from the maturity based heat rate using Eq. 5:

$$\frac{\partial q}{\partial t} = \frac{\partial q}{\partial M} \cdot \frac{\partial M}{\partial t} \qquad (5)$$

where M is the maturity of the concrete at a particular point in the structure and at a particular time after placing the concrete. This means that it is important to monitor the rate of change of maturity at different points of analysis in the structure. A more complete explanation of this approach is presented in Ref. [1].

In order to express the heat-rate curve in generic form, it is proposed that the curve is simplified to the form as shown in Fig. 5. In this form, the curve can be divided into three phases, based on the time of occurrence of the maximum rate of heat evolution. In phase 1, the heat rate function is taken to be linear, starting from a zero heat rate and continuing to the time of occurrence of the peak heat rate plateau (t_1). In this case, the initial peak heat rate, which occurs soon after mixing as a result of the early hydration of the aluminate phases, is ignored. This is justified because, in an actual structural application, this first peak will generally occur before the concrete is placed into the formwork and compacted and will,



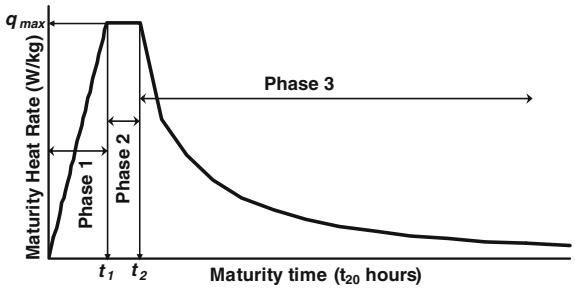


Fig. 5 Simplified heat rate curve

therefore, have little influence on the subsequent temperature development of the concrete.

In Phase 2, the heat rate is taken as constant and equal to the maximum heat rate (q_{max}) over the period between maturity times t_1 and t_2. In Phase 3, the heat rate decays exponentially, starting from maximum heat rate at maturity time t_2. For each of the three phases, the heat rate functions are determined as shown in Eqs. 5–7.

$$Phase\ 1: \quad q_t = q_{max}\frac{t}{t_1} \quad for\ 0 \le t \le t_1 \tag{6}$$

$$Phase\ 2: \quad q_t = q_{max} \quad for\ t_1 < t \le t_2 \tag{7}$$

$$Phase\ 3: \quad q_t = A(t)^B \quad for\ t > t_2 \tag{8}$$

.

For the concretes and binder types tested in this investigation, Table 4 presents values for the coefficients and exponents to be used in Eqs. 6–8. Values of t_1 and t_2 were determined by extrapolating a best-fit line from the rising and declining limbs of the heat curves shown in Figs. 1, 2 and 3. This approach is similar to that proposed by Wang and Dilger [16] except that Eqs. 6–8 are expressed in maturity form.

As an indication of the accuracy of this approach to determining the heat rate curve, Fig. 6 shows a comparison of the measured and predicted heat rates for the different concretes assessed in this investigation, over full temperature measurement periods of up to 320 t_{20} h. The correlation coefficient (R^2) for the data shown in Fig. 6 was calculated as 0.957.

Table 4 Parameter values to be used in Eqs. 5–7 for the different binder types tested

Binder type	q_{max} (W/kg)	t_1 (t_{20} h)	t_2 (t_{20} h)	A	B
100% CEM I	2.80	11.1	17.6	197.5	−1.552
20% GGBS	2.39	11.7	15.3	109.5	−1.391
40% GGBS	1.81	10.0	15.8	143.5	−1.588
60% GGBS	1.30	11.5	14.2	67.4	−1.402
80% GGBS	0.70	10.3	11.0	7.3	−0.937
20% FA	2.11	11.0	16.2	1147.4	−2.146
40% FA	1.57	11.5	16.8	1735.8	−2.366
60% FA	1.07	13.1	17.4	2908.8	−2.665
80% FA	0.70	19.6	22.0	15.5	−1.136
5% CSF	2.71	14.3	17.9	403.9	−1.757
10% CSF	2.80	14.3	14.8	741.1	−1.930
15% CSF	3.05	14.3	15.3	451.0	−1.795

5 Conclusions

The intention of the project reported in this paper was to quantify the effects of supplementary cementing materials on the rate of heat evolution in Portland cement concretes. In particular, the focus was on providing information on the rate of heat evolution in a way that would allow improved prediction of the internal concrete temperature profiles during construction of large or high-strength concrete elements. In this regard and given the parameters of the concretes used, the study has shown that:

- The peak rate of heat evolution in GGBS or FA blended binders decreases linearly with increasing addition of GGBS or FA;
- Except for FA replacements as high as 80%, the time to reach peak rates of heat evolution is reduced with increased proportions of GGBS or FA in the binders. If the proportion of fly ash is increased to 80%, there is a significant increase in the time required to reach the peak rate of heat evolution.
- Up to a replacement level of 15%, the addition of CSF in Portland cement binders does not significantly alter the heat-rate profile of concrete. The most significant effect noted was an approximately 9% increase in the peak rate of hydration when 15% of the Portland cement was replaced by CSF. However, the addition of 10% and 15% CSF had a marked effect in reducing the time to reach the peak rate of hydration.
- The presence of the SCM's assessed in this investigation have the effect of stimulating the hydration of the CEM I in the blended binder.

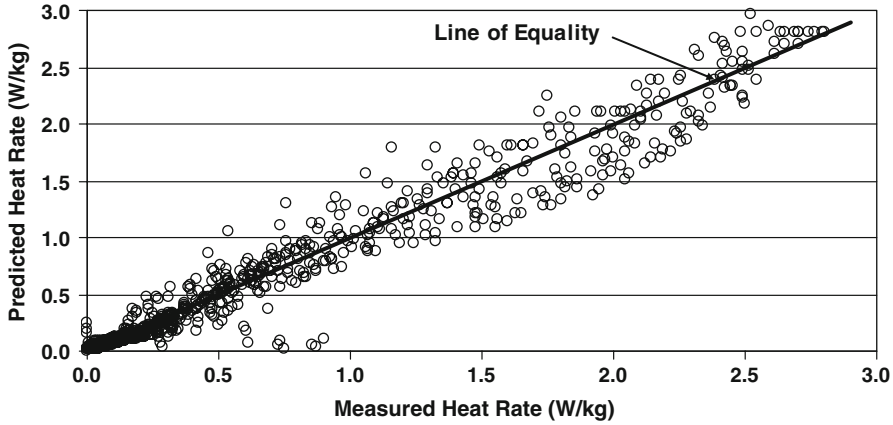


Fig. 6 Accuracy of prediction of the proposed approach to determining the heat rate profile of concrete

This stimulated hydration results from the consumption of calcium hydroxide, the dilution effect and hydration nucleation site effect. This stimulation of hydration is strongest with the addition of CSF, moderate in the case of GGBS and weak in the case of FA.

- In the absence of a more reliable heat-rate curve for concrete containing supplementary cementitious materials, the model proposed in Eqs. 6–8 can be used to provide a first-estimate of the temperature profiles at the design stage of a temperature-sensitive concrete structure.

Acknowledgements The authors wish to express their gratitude to the South African cement industry, Cement and Concrete Institute, Eskom and the National Research Foundation (South Africa) for their financial and logistical support of this project.

References

1. Ballim Y, Graham PC (2003) A maturity approach to the rate of heat evolution in concrete. Mag Concr Res 55(3). doi:10.1680/macr.55.3.249.37571
2. Koenders EAB, van Breugel K (1994) Numerical and experimental adiabatic hydration curve determination. In: Springenschmid R (ed) Thermal cracking in concrete at early ages. E&FN Spon, London
3. Maekawa K, Chaube R, Kishi T (1999) Modelling of concrete performance. Spon Press, London
4. Gibbon GJ, Ballim Y, Grieve GRH (1997) A low cost, computer-controlled adiabatic calorimeter for determining the heat of hydration of concrete. ASTM J Test Eval 25(2):261–266
5. SABS EN 197-1 (2000) Cement—part 1: composition, specifications and conformity criteria for common cements. South African Bureau of Standards, Pretoria
6. SABS 1491-Part 1 (1989) Portland cement extenders, part 1, ground granulated blastfurnace slag. South African Bureau of Standards, Pretoria
7. SABS 1491-Part 2 (1989) Portland cement extenders, part 2 fly ash. South African Bureau of Standards, Pretoria
8. SABS 1491-Part 3 (1989) Portland cement extenders, part 3, condensed silica fume. South African Bureau of Standards, Pretoria
9. Wu X, Roy DM, Langton CA (1983) Early stage hydration of slag-cement. Cem Concr Res 13:277–286. doi:10.1016/0008-8846(83)90111-4
10. Escalante-Garcia JI, Sharp JH (1998) Effects of temperature on the hydration of the main clinker phases in Portland cement: part II, blended cements. Cem Concr Res 28:1259–1274. doi:10.1016/S0008-8846(98)00107-0
11. Zhou J, Ye K, van Breugel K (2006) Hydration of Portland cement blended with blast furnace slag at early stage. 2nd international symposium on advances in concrete science and engineering, Quebec City, Canada. RILEM Publications (on CD)
12. Roy DM (1987) Hydration of blended cements containing slag, fly ash or silica fume. Lecture presented to the Institute of Concrete technology, London
13. Fajun W, Grutzeck MW, Roy DM (1985) The retarding effects of fly ash upon the hydration of cement pastes: the first 24 hours. Cem Concr Res 15:174–184. doi:10.1016/0008-8846(85)90024-9
14. Holman JP (1990) Heat transfer, 7th edn. McGraw Hill Inc, New York
15. Ballim Y (2004) A numerical model and associated calorimeter for predicting temperature profiles in mass concrete. Cem Concr Compos 26(26):695–703
16. Wang C, Dilger WH (1994) Prediction of temperature distribution in hardening concrete. In: Springenschmid R (ed) Thermal cracking in concrete at early ages. E&FN Spon, London